Optica Applicata, Vol. XLIII, No. 4, 2013
DOI: 10.5277/oa130417

Reflection, transmission and ellipsometric parameters of the multilayer structure using a bi-characteristic-impedance transmission line approach

SOFYAN A. TAYA[1*], MUSTAFA H. ABU NASR[2], TAHER M. EL-AGEZ[1]

[1]Physics Department, Islamic University of Gaza, Gaza, Palestine

[2]Faculty of Engineering and Information Technology, Al Azhar University, Gaza, Palestine

[*]Corresponding author: staya@iugaza.edu.ps

Ellipsometry is a powerful tool for studying the optical properties of multilayer structures. All the information extracted from an ellipsometer is found in two angles called the ellipsometric parameters ψ and Δ. The transfer matrix approach is usually used to find the reflectance, transmittance, and ellipsometric parameters of planar multilayer structures. In this work, an equivalent model based on the bi-characteristic-impedance transmission line (BCITL) is employed to model planar multilayer structures. We here apply the BCITL formalism to investigate the reflectance of electromagnetic waves from an isotropic multilayer structure. Moreover, the ellipsometric parameters ψ and Δ for any number of layers are calculated using the BCITL approach. The properties of a Bragg reflector are also presented.

Keywords: bi-characteristic-impedance transmission line, reflectance, Bragg reflector, ellipsometry.

1. Introduction

Planar multilayer structures have received an increasing interest from physicists and engineers due to a wide range of possible applications in electromagnetics; *e.g.*, in the areas of optics, remote sensing, and geophysics [1–5]. The transfer matrix formalism employing the layer and interface matrices is usually used to solve problems related to planar multilayer structures [6]. Another efficient approach called the polynomial one has been applied for treatment of stratified isotropic and anisotropic planar structures [7–9]. In this technique, the reflectance and the transmittance of stratified structures are written in a compact form using the so-called elementary symmetric functions that are extensively used in the mathematical theory of polynomials. These problems can also be solved by modeling these structures using multi-section transmission lines with appropriate characteristic impedances and propagation constants, where each transmission line possesses the same length as of the corresponding layer [5, 10].

Ellipsometry has been extensively used for material and thin film characterization [11–19]. It measures the changes in the state of polarization of light upon reflection or transmission from a sample. The first generations of ellipsometers were single wavelength instruments. With the emergence of spectroscopic ellipsometry, the ellipsometry technique became of high importance to wide research areas from semiconductors to organic materials. Recent developments in spectroscopic ellipsometry have further allowed the real-time characterization of film growth and evaluation of optical anisotropy. The ellipsometric results are usually presented in terms of two parameters ψ and Δ given by

$$\rho = \tan(\psi)\exp(i\Delta) = \frac{r^p}{r^s} \tag{1}$$

where r^p and r^s are the complex Fresnel reflection coefficients for *p*- and *s*-polarized light, respectively.

In this article, the bi-characteristic impedance transmission line (BCITL) approach is employed to model stratified planar structures. Generally, BCITLs are lossy, and possess different characteristic impedances $Z_{0\mathrm{b}}^{\pm}$ of waves propagating in opposite directions. It should be pointed out that BCITLs can be practically implemented using finite lossy periodically loaded transmission lines, and a graphical tool, known as a generalized *T*-chart, has been recently developed for solving problems associated with BCITLs [5]. We here apply the BCITL approach for the study of reflectance of electromagnetic waves from isotropic multilayer structure. The results are compared with those obtained from the well-known matrix formalism. The properties of a Bragg reflector are also investigated. The ellipsometric parameters ψ and Δ for any number of layers are calculated using the BCITL approach.

2. Theory

2.1. Matrix formalism

The addition of a multiple reflection approach is generally used to treat reflection and transmission from a multilayer structure comprising a few number of layers. This approach becomes impractical when treating oblique incidence by a multilayer structure of large number of layers between semi-infinite ambient and substrate media. In such a case, the transfer matrix approach is more effective. In the following, we put forward the matrix formalism in brief although it is presented in details in Refs. [6–9] but it should be mentioned here for the sake of clarity.

A multilayer structure consisting of a stack of *m* parallel, linear, homogeneous, and isotropic layers is sandwiched between two semi-infinite ambient (0) and substrate ($m + 1$) media as shown in Fig. 1. The *j*-th medium has l_j and n_j as a thickness and a refractive index, respectively. The *j*-th interface located at z_j separates the two media of refractive indices n_j and n_{j+1}. An incident wave in medium 0 (the ambient) generates a resultant reflected wave in the same medium and a resultant transmitted wave in

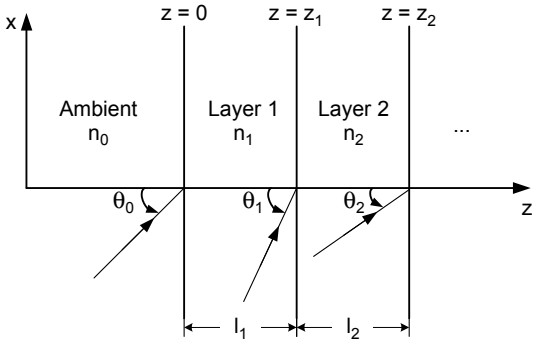

Fig. 1. Oblique incidence on a planar multilayer structure.

medium $m+1$ (the substrate). The total field inside any layer consists of two waves: a forward-traveling wave denoted by "+", and a backward-traveling wave denoted by "–". The total field is usually written as

$$E(z) = \begin{pmatrix} E^{+}(z) \\ E^{-}(z) \end{pmatrix} \tag{2}$$

Considering the fields between the two parallel planes at z' and z'', one can write

$$E(z') = M\,E(z'') \tag{3}$$

where M is the transformation matrix between the planes at z' and z''.

By choosing z' and z'' to lie immediately on the opposite sides of an interface, located at z_j between layers j and $j+1$, Eq. (3) becomes

$$E^{\alpha}(z_j - \delta) = \left[r_j^{\alpha}\right] E^{\alpha}(z_j + \delta) \tag{4}$$

where δ is an infinitely small distance, $\alpha = p$ or s indicating the state of polarization, and $[r_j^{\alpha}]$ is called the interface matrix which is given by

$$\left[r_j^{\alpha}\right] = \frac{1}{t_{j,j+1}^{\alpha}} \begin{bmatrix} 1 & r_{j,j+1}^{\alpha} \\ r_{j,j+1}^{\alpha} & 1 \end{bmatrix} \tag{5}$$

where $r_{j,j+1}$ and $t_{j,j+1}$ are Fresnel reflection and transmission coefficients at the $j, j+1$ interface.

On the other hand, if z' and z'' are chosen inside the j-th layer at its boundaries, Eq. (3) becomes

$$E^{\alpha}(z_{j-1} + \delta) = [\phi_j]\, E^{\alpha}(z_j - \delta) \tag{6}$$

where $[\phi_j]$ is called the layer matrix which is given by

$$[\phi_j] = \begin{pmatrix} e^{i\varphi_j} & 0 \\ 0 & e^{-i\varphi_j} \end{pmatrix} \tag{7}$$

where $\varphi_j = k n_j \cos(\theta_j l_j)$ with $k = \omega/c$ is the free space wave number and θ_j is the refraction angle in the j-th layer.

The M-matrix for the whole structure can be expressed as a product of the interface and layer matrices that describe the effects of the individual interfaces and layers of the entire stratified structure, taken in proper order, as follows

$$\left[M_N^{\alpha}\right] = \left[\phi_1\right]\left[r_1^{\alpha}\right]\left[\phi_2\right]\left[r_2^{\alpha}\right]\ldots\left[\phi_N\right]\left[r_N^{\alpha}\right] \tag{8}$$

For the last interface we have $E_N^- = 0$, so that the reflection and transmission coefficients of the whole system are given by

$$\left.\begin{aligned} r_N^{\alpha} &= \frac{E_1^-}{E_1^+} = \frac{(M_N^{\alpha})_{21}}{(M_N^{\alpha})_{11}} \\ t_N^{\alpha} &= \frac{E_N^+}{E_1^+} = \frac{1}{(M_N^{\alpha})_{11}} \end{aligned}\right\} \tag{9}$$

The reflectance of the structure is given by

$$R = \frac{\left|r_N^p\right|^2 + \left|r_N^s\right|^2}{2} \tag{10}$$

whereas the transmittance is given by $T = (1 - R)$ provided that no absorbance is present.

2.2. Bi-characteristic impedance transmission line (BCITL)

Planar multilayer structure shown in Fig. 1 can be treated by modeling it using multi-section transmission lines. The equivalent multi-section model of Fig. 1 is depicted in Fig. 2, where β_j is the propagation constant and Z_j is the characteristic impedance of each transmission line and they are given by

$$\beta_j = k n_j \cos(\theta_j) \tag{11}$$

$$Z_j = \begin{cases} \eta_j \cos(\theta_j) & \text{for } p\text{-polarized light} \\ \eta_j \sec(\theta_j) & \text{for } s\text{-polarized light} \end{cases} \tag{12}$$

where η_j is the intrinsic impedance of the j-th layer. The multi-section transmission line is assumed to be terminated in surface impedance of Z_S at $z = z_N$. It should be

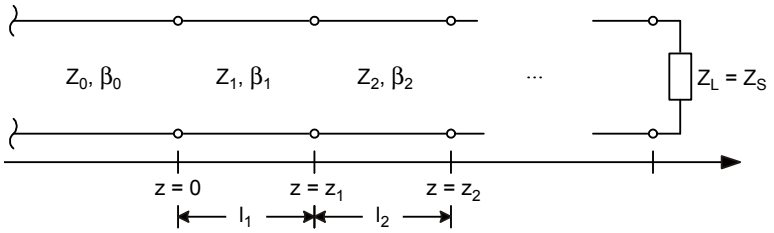

Fig. 2. Multi-section transmission line model.

pointed out that for the lossy case, the propagation constant β_j is a complex number. If the angle θ_j is real and the refractive index n_j of the j-th layer is given by $n_j = n_r + jn_i$, then the real part of β_j is simply given by $\mathrm{Re}(\beta_j) = kn_r\cos(\theta_j)$, whereas the imaginary part is given by $\mathrm{Im}(\beta_j) = kn_i\cos(\theta_j)$. In most cases, θ_j is a complex angle and in this case the real and imaginary parts of β_j are more complicated.

In transmission line analysis, impedance, admittance, scattering and *ABCD* matrices are usually used. Impedance and admittance matrices describe the relationship between the total voltages and currents defined at the terminal ports or interferences of arbitrary *N*-port multi-section transmission lines. The scattering matrix gives an alternative characterization of *N*-port multi-section transmission lines in terms of incident and reflected waves. *ABCD* matrix is known as a transmission matrix [20]. The *ABCD* matrix of a section of transmission line with length l, characteristic impedance Z_0, and propagation constant β is given by

$$\begin{bmatrix} A & B \\ C & D \end{bmatrix} = \begin{bmatrix} \cos(\beta l) & jZ_0\sin(\beta l) \\ j\dfrac{1}{Z_0}\sin(\beta l) & \cos(\beta l) \end{bmatrix} \tag{13}$$

For the cascading *N*-section transmission lines, the total *ABCD* matrix parameters are given by

$$\begin{bmatrix} A & B \\ C & D \end{bmatrix} = \begin{bmatrix} A_1 & B_1 \\ C_1 & D_1 \end{bmatrix}\begin{bmatrix} A_2 & B_2 \\ C_2 & D_2 \end{bmatrix}\cdots\begin{bmatrix} A_N & B_N \\ C_N & D_N \end{bmatrix} \tag{14}$$

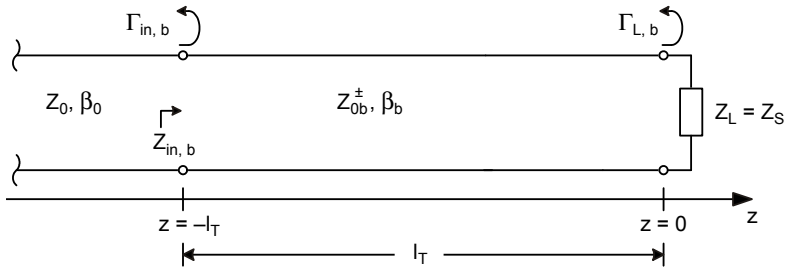

Fig. 3. Transmission line BCITL model.

The multi-section model shown in Fig. 2 can be treated effectively using the BCITL model shown in Fig. 3 where $Z_{0b}^{\pm}$ and β_b are the characteristic impedance and the propagation constant of the equivalent structure, respectively. $\Gamma_{\text{in},\,b}$ and $Z_{\text{in},\,b}$ represent the total input reflection coefficient and the input impedance, respectively. $Z_{0b}^{\pm}$ and β_b and can be determined from the total *ABCD* matrix of the cascading *N*-section transmission line of the total length l_T as [21]

$$Z_{0b}^{\pm} = \frac{\pm jB}{\sqrt{1-(AD)^2}} \tag{15}$$

and

$$\cos(\beta_b l_T) = A = D \tag{16}$$

It should be pointed out here that the two transmission line models shown in Figs. 2 and 3 are equivalent; *i.e.*, their total transmission matrices are identical [5]. This can be shown using the theory of two-port network [20]. It is also worth to mention that the BCITL model is equivalent to the multi-section model at the input and output terminals only; *i.e.*, at $z = 0$ and $z = z_N$, respectively. This is due to the fact that the multi-section transmission line in Fig. 2 is globally viewed as a two-port network in constructing the BCITL model.

It is straightforward to show that the total input reflection coefficient $\Gamma_{\text{in},\,b}$ can be written in terms of the input impedance $Z_{\text{in},\,b}$ as [21]

$$\Gamma_{\text{in},\,b} = \pm\left[\frac{Z_{\text{in},\,b}-Z_0}{Z_{\text{in},\,b}+Z_0}\right] \tag{17}$$

where

$$Z_{\text{in},\,b} = \frac{V(z=-l_T)}{I(z=-l_T)} = Z_{0b}^{+}Z_{0b}^{-}\left[\frac{1+\Gamma_{L,\,b}e^{-j2\beta_b l_T}}{Z_{0b}^{-}-Z_{0b}^{+}\Gamma_{L,\,b}e^{-j2\beta_b l_T}}\right] \tag{18}$$

and

$$\Gamma_{L,\,b} = \frac{Z_S Z_{0b}^{-}-Z_{0b}^{+}Z_{0b}^{-}}{Z_S Z_{0b}^{-}+Z_{0b}^{+}Z_{0b}^{-}} \tag{19}$$

with

$$V(z) = V_0^{+}e^{-j\beta^{+}z}+V_0^{-}e^{-j\beta^{-}z} \tag{20a}$$

$$I(z) = \frac{V_0^{+}}{Z_0}e^{-j\beta^{+}z}-\frac{V_0^{-}}{Z_0}e^{-j\beta^{-}z} \tag{20b}$$

and

$$\Gamma = \frac{V_0^-}{V_0^+} \tag{21}$$

where $\Gamma_{L,b}$ is the load reflection coefficient associated with the BCITL and is defined at $z = z_N$. In Eq. (17), the plus and minus signs correspond to the perpendicular and parallel polarizations, respectively. The minus sign comes from the fact that the total input reflection coefficient is associated with the current, instead of the voltage, for the parallel polarization.

3. Results and discussion

We first investigate the behavior of the characteristic impedance $Z_{0b}^{\pm}$, the propagation constant β_b, and the total input reflection coefficient $\Gamma_{\text{in},b}$ with the angle of incidence. We consider a three-layer structure having the parameters, $l_1 = 1000$ nm, $l_2 = 1200$ nm, $l_3 = 1400$ nm, $\mu_{r,1} = \mu_{r,2} = \mu_{r,3} = 1$, $n_1 = 1.50 - 0.01i$, $n_2 = 1.57 - 0.01i$, $n_3 = 1.59 - 0.01i$, and $Z_s = 50\ \Omega$. The structure is assumed to be illuminated with a He-Ne laser beam ($\lambda = 632.8$ nm) at an incidence angle θ_0 which can be varied from 0 to 90°. The parameters $|Z_{0b}^{\pm}|$, $\arg(Z_{0b}^{\pm})$, β_b, and $|\Gamma_{\text{in},b}^{s}|$ are then calculated and plotted *versus* θ_0 for *s*- and *p*-polarizations as shown in Figs. 4 and 5, respectively. As can be seen from the figures, Z_{0b}^{+} and Z_{0b}^{-} are generally complex and different from each other because the structure is assumed to be lossy. Moreover, $Z_{0b}^{\pm}$ is polarization dependent. The propagation constant β_b is also complex and has a significant

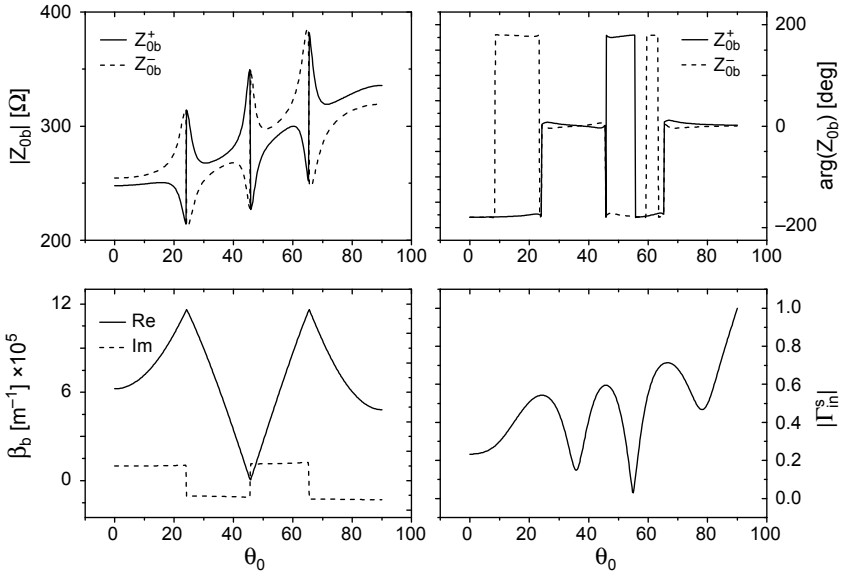

Fig. 4. $|Z_{0b}^{\pm}|$, $\arg(Z_{0b}^{\pm})$, β_b, and $|\Gamma_{\text{in},b}^{s}|$ *versus* the incidence angle θ_0 for *s*-polarized waves for three-layer structure.

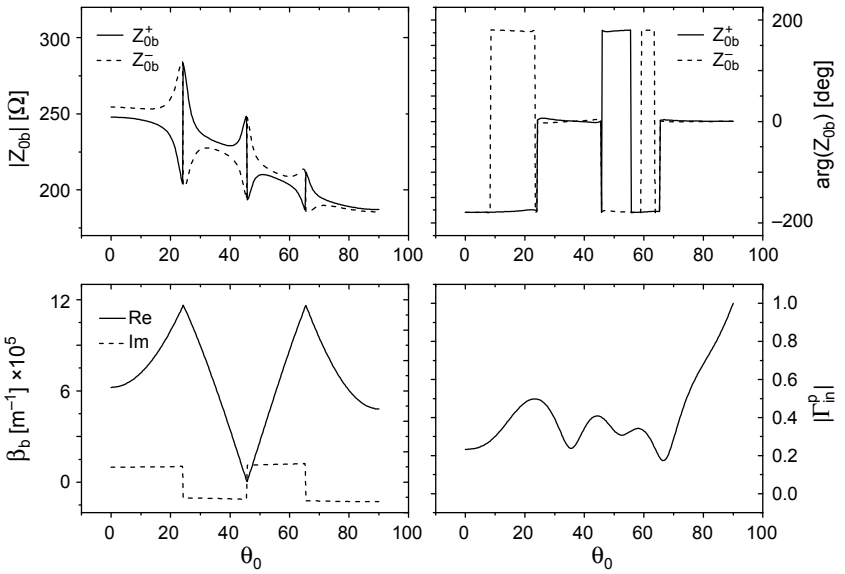

Fig. 5. $|Z_{0b}^{\pm}|$, $\arg(Z_{0b}^{\pm})$, β_b, and $|\Gamma_{\text{in},\,b}^{p}|$ *versus* the incidence angle θ_0 for *p*-polarized waves for three-layer structure.

dependence on the incidence angle. Moreover, the magnitude of the total input reflection coefficient varies considerably with θ_0 and with the type of the light polarization.

To demonstrate the validity of the BCITL approach, we consider a planar multilayer dielectric coating designed as a Bragg reflector. Bragg reflectors are composed of multiple thin layers of dielectric material, typically deposited on a substrate of glass. Through proper choice of the thickness and refractive indices of the dielectric layers, it is possible to design an optical coating with specified reflectance at different light wavelengths. Moreover, Bragg reflectors can be used to fabricate ultra-high reflectivity mirrors over a narrow range of wavelengths. Alternatively, they can be made to reflect a broad spectrum of light. Bragg reflectors have found a wide range of applications such as laser thin-film beam-splitters, cavity end mirrors, and hot and cold mirrors. The function of operation of Bragg reflectors is based on the interference of light reflected from the stack of dielectric layers. The Bragg reflector usually consists of identical alternating layers of high and low refractive indices. The optical thicknesses are typically chosen to be quarter-wavelength long at some center wavelength λ_0, that is, $n_H l_H = n_L l_L = \lambda_0/4$, where n_H and n_L are the indices of refraction of the high- and low-index layers, respectively, l_H and l_L are the thicknesses of the high- and low-index layers, respectively. The standard arrangement is to have an odd number of layers, with the high index layer being the first and last layer [22].

The numerical calculations are conducted for a system of odd number of layers of quarter-wavelength layers. The design wavelength of the Bragg reflector is centered

at 550 nm since our calculations were done in the spectral range from 350–850 nm. We also consider TiO_2 and MgF_2 as high-index and low-index dielectrics, respectively, and the substrate is glass. The optical parameters of these materials were obtained from the handbook of optical constants of solids [23]. TiO_2 and MgF_2 are found to have the refractive index ranges 4.005–2.78 and 1.387–1.375, respectively, in the spectral range 350–850 nm. The calculated total input reflection coefficient $\Gamma_{\text{in},\,b}$ for *s*- and *p*-polarizations using the BCITL for 7 layer-quarter-wavelength Bragg reflector at $\theta_0 = 20°$ is shown in Fig. 6. The figure also shows the total reflectance calculated using the matrix approach, Eq. (10), and using the BCITL using *R*:

$$R = \frac{\left|\Gamma^{p}_{\text{in},\,b}\right|^2 + \left|\Gamma^{s}_{\text{in},\,b}\right|^2}{2}$$

It is found that the equivalent BCITL model provides identical results, for both *s*- and *p*-polarizations, as those obtained from the propagation matrix approach.

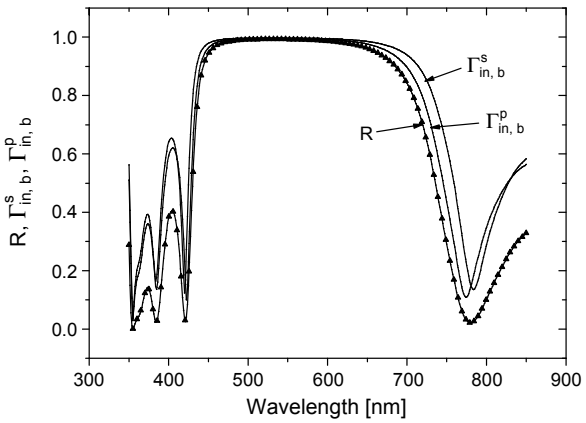

Fig. 6. Calculated $\Gamma^{p}_{\text{in},\,b}$, $\Gamma^{s}_{\text{in},\,b}$ and *R* of 7 layer-quarter-wavelength Bragg reflectors at $\theta_0 = 20°$ using the BCITL approach (lines) and the matrix approach (points).

Moreover, we investigate the behavior of the reflectance from the Brag reflector for the cases of 3, 7, and 15 layers using the BCITL approach as shown in Fig. 7. As the number of layers increase, the reflectance rises and becomes flatter within the bandwidth $\Delta\lambda$. Also it has sharper edges and tends to 100%. This is a consequence of the periodic nature of the Bragg reflector.

To study the ellipsometric parameters ψ and Δ for the 3, 7, and 15 layer Bragg reflector, we consider $\theta_0 = 70°$ since most of the ellipsometric devices are operated at this incidence angle. The importance of ψ and Δ comes from the fact that once they are determined during a measurement at a given wavelength, one can invert Fresnel equations to extract the optical parameters of a bulk sample. For a multilayer structure one must perform a spectroscopic ellipsometric scan over a certain spectrum to

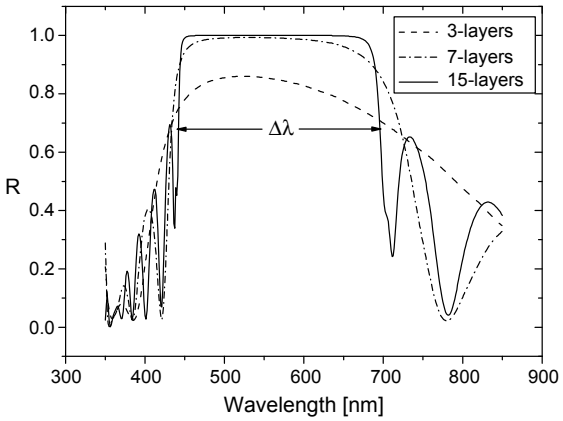

Fig. 7. Calculated reflectance R of 3, 7, and 15 layer-quarter-wavelength Bragg reflectors at $\theta_0 = 20°$ using the BCITL approach.

determine the thickness, the refractive index, and the extinction factor for each layer. Figures 8 and 9 show respectively ψ and Δ for the 3, 7, and 15 layer Bragg reflector in the spectral range 350–850 nm. As the figures reveal, ψ ranges between 1°–47° whereas Δ ranges between 0–358°. Both of them change considerably with the number of layers constituting the Bragg reflector. As can be seen from Fig. 8, the behavior of ψ with the wavelength for the 3, 7, and 15 layer Bragg reflector is very close to that of the reflectance. As the number of layers increases, ψ rises and becomes flatter within some bandwidth. Also it has sharper edges and tends to 45° which means the complex Fresnel reflection coefficients for *p*- and *s*-polarized lights have equal magnitudes. In the spectral regions $\lambda < 410$ nm and $\lambda > 575$ nm, the ellipsometric parameter ψ oscillates between 0 and 45°.

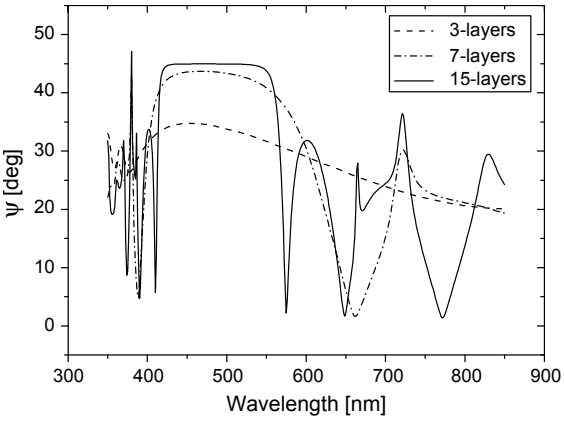

Fig. 8. The ellipsometric parameter ψ of 3, 7, and 15 layer-quarter-wavelength Bragg reflectors at $\theta_0 = 70°$ in the spectral range of 350–850 nm using the BCITL approach.

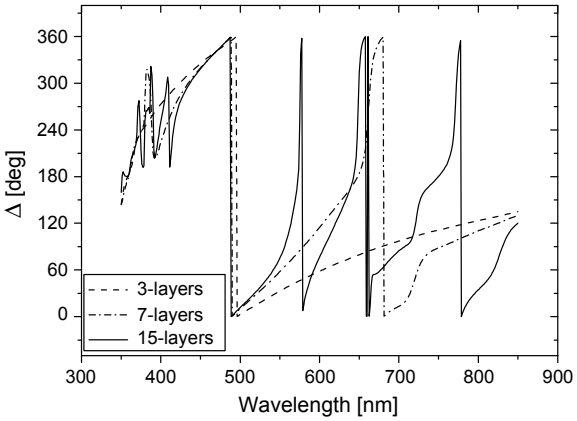

Fig. 9. The ellipsometric parameter Δ of 3, 7, and 15 layer-quarter-wavelength Bragg reflectors at $\theta_0 = 70°$ in the spectral range of 350–850 nm using the BCITL approach.

Finally, it is very significant to use the BCITL to study the influence of the refractive index ratio n_L/n_H on the reflectance spectrum. Reflectance spectrum of different refractive index ratios of 15 layer-quarter-wavelength Bragg reflector at $\theta_0 = 0°$ (normal incidence) is depicted in Fig. 10. The refractive index ratio n_L/n_H is 1.5/2, 1.5/2.5, 1.5/3, and 1.5/3.5. This ratio has a great influence on the bandwidth and the sharpness of reflectance curves. From Fig. 10 we can conclude that the increase in the ratio n_L/n_H leads to the widening of the bandwidth. For example, for $n_L/n_H = 1.5/2$ the bandwidth is about 130 nm whereas for $n_L/n_H = 1.5/3.5$ it is about 330 nm. Another important effect that can be seen from the figure is the sharpness of the band edges. The band edges become sharper when the ratio increases. An interesting feature can be seen from Fig. 10 which is the asymmetry of these spectra

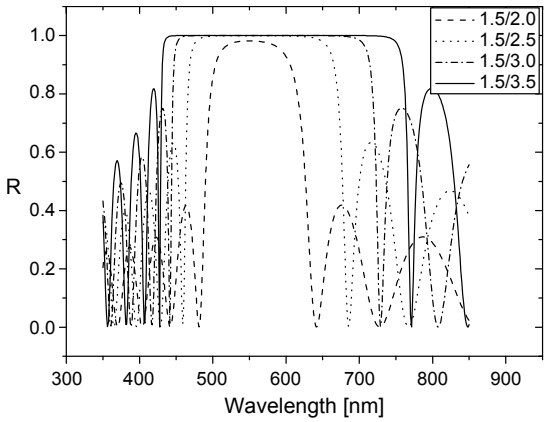

Fig. 10. Reflectance spectrum of 15 layer-quarter-wavelength Bragg reflectors at $\theta_0 = 0$ using the BCITL approach for different n_L/n_H ratio.

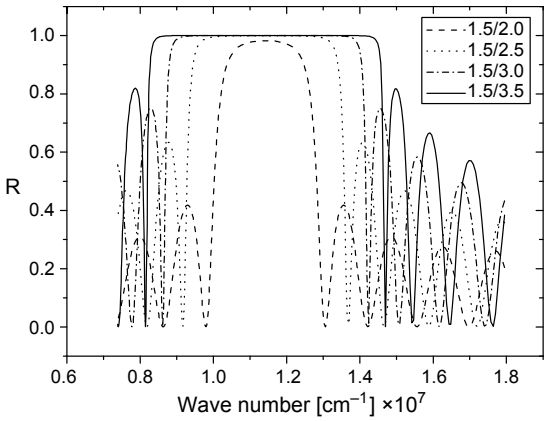

Fig. 11. Reflectance spectrum of 15 layer-quarter-wavelength Bragg reflectors at $\theta_0 = 0$ using the BCITL approach. In this case, the wave number is used as *x*-axis.

around the central wavelength. The curves are shifted to the left with decreasing the ratio n_L/n_H. The symmetry can be observed when the magnitude of the *x*-axis is wave number instead of wavelength as shown in Fig. 11.

4. Conclusions

A simple method based on an equivalent model of the bi-characteristic-impedance transmission line is proposed to model planar multilayer structures. The ellipsometric parameters ψ and Δ and the reflectance for any number of Bragg reflector layers have been studied in details using this simple approach. The results obtained are identical with those extracted from the propagation matrix approach.

References

[1] KHALAJ-AMIRHOSSEINI M., *Analysis of lossy inhomogeneous planar layers using Taylor's series expansion*, IEEE Transactions on Antennas and Propagation **54**(1), 2006, pp. 130–135.

[2] KHALAJ-AMIRHOSSEINI M., *Analysis of lossy inhomogeneous planar layers using the method of moments*, Journal of Electromagnetic Waves and Applications **21**(14), 2007, pp. 1925–1937.

[3] AISSAOUI M., ZAGHDOUDI J., KANZARI M., REZIG B., *Optical properties of the quasi-periodic one-dimentional generalized multilayer Fibonacci structures*, Progress in Electromagnetics Research **59**, 2006, pp. 69–83.

[4] YILDIZ C., TURKMEN M., *Quasi-static models based on artificial neural networks for calculating the characteristic parameters of multilayer cylindrical coplanar waveguide and strip line*, Progress in Electromagnetics Research B **3**, 2008, pp. 1–22.

[5] TORRUNGRUENG D., LAMULTREE S., *analysis of planar multilayer structures at oblique incidence using an equivalent BCITL model*, Progress in Electromagnetics Research C **4**, 2008, pp. 13–24.

[6] AZZAM R.M., BASHARA N.M., *Ellipsometry and Polarized Light*, North-Holland, Amsterdam, 1977.

[7] SHABAT M.M., TAYA S.A., *A new matrix formulation for one-dimensional scattering in Dirac comb (electromagnetic wave approach)*, Physica Scripta **67**(2), 2003, pp. 147–152.

[8] EL-AGEZ T., TAYA S., EL TAYAYN A., *A polynomial approach for reflection, transmission, and ellipsometric parameters by isotropic stratified media*, Optica Applicata **40**(2), 2010, pp. 501–510.
[9] TAYA S.A., EL-AGEZ T.M., *Ellipsometry of anisotropic materials: a new efficient polynomial approach*, Optik **122**(8), 2011, pp. 666–670.
[10] WAIT J.R., *Electromagnetic Wave Theory*, John Wiley & Son, Sigapore, 1989.
[11] FUJIWARA H., *Spectroscopic Ellipsometry Principles and Applications*, John Wiley & Sons, West Sussex, 2007.
[12] EL-AGEZ T.M., EL TAYYAN A.A., TAYA S.A., *Rotating polarizer-analyzer scanning ellipsometer*, Thin Solid Films **518**(19), 2010, pp. 5610–5614.
[13] EL-AGEZ T.M., TAYA S.A., *A Fourier ellipsometer using rotating polarizer and analyzer at a speed ratio 1:1*, Journal of Sensors, 2010, article 706829.
[14] EL-AGEZ T.M., TAYA S.A., *An extensive theoretical analysis of the 1:2 ratio rotating polarizer–analyzer Fourier ellipsometer*, Physica Scripta **83**(2), 2011, article 025701.
[15] EL-AGEZ T.M., TAYA S.A., *Development and construction of rotating polarizer analyzer ellipsometer*, Optics and Lasers in Engineering **49**(4), 2011, pp. 507–513.
[16] EL-AGEZ T.M., TAYA S.A., EL TAYYAN A.A., *An improvement of scanning ellipsometer by rotating a polarizer and an analyzer at a speed ratio of 1:3*, International Journal of Optomechatronics **5**(1), 2011, pp. 51–67.
[17] EL-AGEZ T.M., WIELICZKA D.M., MOFFITT C., TAYA S.A., *Spectroscopic ellipsometry time study of low-temperature plasma-polymerized plain trimethylsilane thin films deposited on silicon*, Physica Scripta **84**(4), 2011, article 045302.
[18] TAYA S.A., EL-AGEZ T.M., ALKANOO A.A., *Thin film characterization using rotating polarizer analyzer ellipsometer with a speed ratio 1:3*, Journal of Electromagnetic Analysis and Applications **3**(9), 2011, pp. 351–358.
[19] EL-AGEZ T.M., WIELICZKA D.M., MOFFITT C., TAYA S.A., *Aging of oxygen treated trimethylsilane plasma polymerized films using spectroscopic ellipsometry*, Journal of Atomic and Molecular Physics, 2011, article 295304.
[20] POZAR D.M., *Microwave Engineering*, Wiley, NJ, 2005.
[21] TORRUNGRUENG D., THIMAPORN C., *A generalized ZY Smith chart for solving nonreciprocal uniform transmission-line problems*, Microwave and Optical Technology Letters **40**(1), 2004, pp. 57–61.
[22] ORFANIDIS S.J., *Electromanetic Waves and Antennas*, on-line textbook, Rutgers University, http://www.ece.rutgers.edu/~orfanidi/ewa
[23] PALIK E., *Handbook of Optical Constants of Solids*, Academic Press, San Diego, CA, 1998.

Received April 11, 2013
in revised form July 8, 2013